

# Evolution of different orders of coherence of a three-qubit system and their protection via dynamical decoupling on an NMR quantum processor

Akanksha Gautam,<sup>1,\*</sup> Kavita Dorai,<sup>1,†</sup> and Arvind<sup>1,‡</sup>

<sup>1</sup>*Department of Physical Sciences, Indian Institute of Science Education & Research Mohali, Sector 81 SAS Nagar, Manauli PO 140306 Punjab India.*

We generate different orders of quantum coherence in a three-qubit NMR system and study their dynamics in the presence of inherent noise. Robust dynamical decoupling (DD) sequences are applied to preserve the different coherence orders. Initially, DD sequences are implemented simultaneously on all three spins, which effectively protects third-order coherence; however, other coherence orders decay rapidly instead of being preserved. The robust DD sequences were suitably modified in order to preserve other coherence orders. These sequences are applied to the two participating qubits that generate each zero and second order coherence, ensuring their effective preservation. In contrast, first-order coherence is preserved more efficiently when DD sequences are applied exclusively on the qubit responsible for generating it. Instead of performing full state tomography, coherence orders are measured directly using single pulses. The robust DD protection schemes are finally applied to successfully protect two-qubit entanglement in three-qubit star states.

## I. INTRODUCTION

Quantum coherence, quantum entanglement and other quantum correlations are key consequences of the principle of quantum superposition which distinguishes quantum mechanics from classical theory [1]. The generation and maintenance of quantum coherence are essential in novel quantum information processing (QIP) schemes [2, 3], quantum metrology [4], quantum thermodynamics [5–7], solid state physics [8], NMR quantum QIP [9, 10] and QIP based on superconducting systems [11, 12]. Quantum coherence also plays a prominent role in quantum phenomena observed in photosynthesis and avian magnetic navigation [13–16].

While quantum coherence is an essential component in QIP, significant advancements in its theory have been developed only recently [17]. Subsequently, coherence has been studied in different contexts including freezing coherence [18], direct measurement using witness operators and entanglement [19, 20], partial coherence and its connection to entanglement [21], transforming coherence into quantum correlations [22] and coherence distillation [23, 24]. These quantifiers only reflect the total amount of coherence in a quantum state, which may not provide complete information, as discussed in [25]. While a single-qubit system can demonstrate quantum coherence, quantum correlation necessitate the interaction of at least two qubits, which are linked through higher-order coherences [26]. Within the context of NMR, quantum coherence is characterized by coherence order, which relates to the transitions between eigenstates [27].

The interaction of quantum coherence with environmental noise causes it to gradually degrade over time, ultimately leading to decoherence. Hence, a signifi-

cant challenge in developing practical quantum computers is to control environmental noise in order to preserve quantum coherence for extended durations. The impact of decoherence can be mitigated through various previously proposed techniques, such as the quantum Zeno effect [28], quantum weak measurements [29, 30], quantum error correction codes [31], decoherence-free subspaces [32], and dynamical decoupling (DD) sequences [33–36]. Several experimental schemes to preserving quantum coherence have been demonstrated using different quantum technologies [37–41]. Amongst all proposed coherence protection strategies, DD sequences have proven to be very successful in protecting single-qubit quantum states [42, 43] and several DD sequences have been successfully implemented to preserve entanglement in two NMR qubits and to freeze quantum discord in a dephasing noisy NMR environment [44, 45].

In this work, we experimentally investigated the dynamics of various orders of coherence (zeroth, first, second and third order) as they evolve under the natural environmental noise present in an NMR system. Several three-qubit quantum states were experimentally generated, each exhibiting distinct orders of coherence. These coherence orders are also connected to quantum correlations; for instance, tripartite correlation is linked to third-order coherence, while zeroth and second-order coherence are associated with bipartite correlations. Subsequently, the quantum states were protected using DD sequences, with each coherence order being protected to an different extent. While some coherences are preserved to a certain extent by the robust DD sequence, others deteriorate rapidly instead of being preserved. Hence, new modified robust DD sequences were designed and utilized to protect each order of coherence. To protect third-order coherence, robust DD sequences were simultaneously applied to all three nuclear spins, resulting in their protection for a certain duration. First-order coherence was effectively protected through the application of a robust DD sequence on the single qubit responsible for creat-

\* akanksha.gautam512@gmail.com

† kavita@iisermohali.ac.in

‡ arvind@iisermohali.ac.in

ing that coherence. Modified robust DD sequences were successfully applied to the two qubits involved in generating zeroth and second-order coherences, and the results demonstrate successful preservation of both zeroth and second-order coherence. Subsequently, the effectiveness of all four robust DD sequences in preserving different orders of coherence was compared. Star states have all possible coherence orders and correlations present and have been shown to be useful for quantum error correction [46]. Hence, a three-qubit star state was created and the entanglement in its two-qubit subsystems was protected using a modified version of a robust DD sequence.

This paper is organized as follows: Section II provides a brief description of different coherence orders, and outlines the entanglement structure of the three-qubit star state. Protection schemes based on robust DD sequences are described in Section III. The experimental details and results of implementing robust DD sequences to protect zero-order, first-order, second-order, and third-order coherences are presented in Sections IV A-IV D, respectively. Section V discusses experiments performed to protect the entanglement of a two-qubit subsystem within the three-qubit star state, while Section VI contains a few concluding remarks.

## II. COHERENCE ORDERS AND STAR STATE ENTANGLEMENT

In this section, we describe various coherence orders and star states which will be experimentally generated and protected using DD sequences.

### A. Coherence orders

Coherence orders in an NMR system are linked to transitions among various energy levels, each defined by specific quantum numbers [47, 48]. For instance, first-order quantum coherence is observed when the transition between two eigenstates yields a quantum number of 1, whereas maximal coherence order occurs when the transition takes place between the ground state and the highest energy state. The populations of each energy level are represented by the diagonal elements of the density matrix of the system, whereas coherence of different orders are represented by the off-diagonal elements. In matrix form, the various coherence orders found in a three-qubit system are depicted by the elements shown below, where the elements highlighted in red represent the coherence orders that were experimentally created in this work.

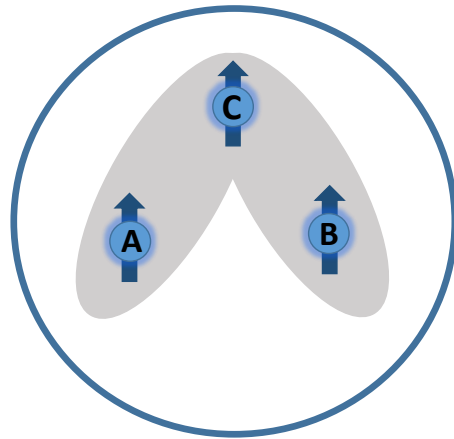


FIG. 1. Entanglement arrangement of a three-qubit star state is represented by a circle, indicating that all three qubits are genuinely entangled with one another, while the specific pairs of qubits that exhibit entanglement are marked by the grey-shaded regions.

$$N = \begin{pmatrix} 0 & +1 & +1 & +2 & +1 & +2 & +2 & +3 \\ -1 & 0 & 0 & +1 & 0 & +1 & +1 & +2 \\ -1 & 0 & 0 & +1 & 0 & +1 & +1 & +2 \\ -2 & -1 & -1 & 0 & -1 & 0 & 0 & +1 \\ -1 & 0 & 0 & +1 & 0 & +1 & +1 & +2 \\ -2 & -1 & -1 & 0 & -1 & 0 & 0 & +1 \\ -2 & -1 & -1 & 0 & -1 & 0 & 0 & +1 \\ -3 & -2 & -2 & -1 & -2 & -1 & -1 & 0 \end{pmatrix} \quad (1)$$

(i) **Zero-order coherence:** arises when a transition between two energy levels involves a quantum number of zero, and is associated with bipartite correlations. For instance, transitions that take place between  $|10\rangle \rightarrow |01\rangle$  and  $|010\rangle \rightarrow |101\rangle$ .

(ii) **First-order coherence:** arises when the quantum number associated with the transition between two energy levels is one, and is directly detected according to quantum mechanical selection rules. For instance, transitions occurring between  $|00\rangle \rightarrow |01\rangle$  and  $|010\rangle \rightarrow |011\rangle$ .

(iii) **Second-order coherence:** arises when the transition between two energy levels corresponds to a total quantum number of two where it is associated with the measurement of bipartite correlation. For example, transitions occurring between  $|00\rangle \rightarrow |11\rangle$  and  $|100\rangle \rightarrow |111\rangle$ .

(iv) **Third-order coherence:** is represented by the transition between the ground state and the highest energy level of a three-qubit system, which results in the emergence of third-order coherence (associated with tripartite correlations), characterized by a quantum number of three.

### B. Star States

Genuinely entangled, three-qubit states are categorized into two entanglement classes, namely GHZ and W,

which are not convertible upto stochastic local operations and classical communication (SLOCC). The three-qubit star state, falls under the GHZ class, and exhibits both tripartite and bipartite entanglement [27]. Such states exhibit coherences of all possible orders and are simple examples of graph states which have been shown to be important for several quantum information processing tasks. The entanglement configuration in a three-qubit star state is depicted in Figure 1 and is mathematically expressed as [46]:

$$\begin{aligned} |S_1\rangle &= \alpha_1 |000\rangle + \beta_1 |100\rangle + \gamma_1 |101\rangle + \delta_1 |111\rangle \\ |S_2\rangle &= \alpha_2 |000\rangle + \beta_2 |100\rangle + \gamma_2 |110\rangle + \delta_2 |111\rangle \end{aligned} \quad (2)$$

where the existence of the star state necessitates that the parameters  $\alpha_1, \beta_1, \gamma_1, \delta_1, \alpha_2, \beta_2, \gamma_2$  and  $\delta_2$  are all non-zero. In the context of the entanglement structure of the three-qubit star state, where qubits 1, 2, and 3 are represented by A, B, and C, respectively, there is one central qubit and two peripheral qubits, with the central qubit being entangled with both peripheral qubits. For instance, in the entanglement configuration of the  $|S_1\rangle$  state (Eqn. 2), the central qubit C is entangled with both peripheral qubits A and B, indicating the presence of entanglement in the reduced density matrices  $\rho_{AC}^{S_1}$  and  $\rho_{BC}^{S_1}$ . In contrast,  $\rho_{AB}^{S_1}$  is found to have no entanglement. Similarly, the entanglement structure of the  $|S_2\rangle$  state involves the central qubit B, which is entangled with the peripheral qubits A and C [46]. In this study, we investigate the entanglement structure and coherence orders exhibited by the state  $|S_1\rangle$ . Therefore, we fixed the values of  $\alpha_1, \beta_1, \gamma_1$  and  $\delta_1$  to  $\frac{1}{2}$ , leading to:

$$|\psi^{star}\rangle = \frac{1}{2} (|000\rangle + |100\rangle + |101\rangle + |111\rangle) \quad (3)$$

The density matrix of the three-qubit star state is given by:

$$\rho_{star} = \begin{pmatrix} \frac{1}{4} & 0 & 0 & 0 & \frac{1}{4} & \frac{1}{4} & 0 & \frac{1}{4} \\ 0 & 0 & 0 & 0 & 0 & 0 & 0 & 0 \\ 0 & 0 & 0 & 0 & 0 & 0 & 0 & 0 \\ 0 & 0 & 0 & 0 & 0 & 0 & 0 & 0 \\ \frac{1}{4} & 0 & 0 & 0 & \frac{1}{4} & \frac{1}{4} & 0 & \frac{1}{4} \\ \frac{1}{4} & 0 & 0 & 0 & \frac{1}{4} & \frac{1}{4} & 0 & \frac{1}{4} \\ 0 & 0 & 0 & 0 & 0 & 0 & 0 & 0 \\ \frac{1}{4} & 0 & 0 & 0 & \frac{1}{4} & \frac{1}{4} & 0 & \frac{1}{4} \end{pmatrix} \quad (4)$$

where the blue-highlighted element  $\rho_{18}$  denotes third order coherence (linked to tripartite correlations), while the second order coherences (linked to bipartite correlations) denoted by the red-highlighted elements  $\rho_{16}$  and  $\rho_{58}$  are found in the reduced density matrices  $\rho_{AC}^{star}$  and  $\rho_{BC}^{star}$ , respectively [46]. In this work, concurrence measure is utilized to detect and quantify the existence of entanglement in the subsystems  $\rho_{AC}^{star}$  and  $\rho_{BC}^{star}$ . These two-qubit reduced states are mixed entangled states and concurrence serves as an effective measure of entanglement for mixed states, with both states having a concurrence value of 0.5.

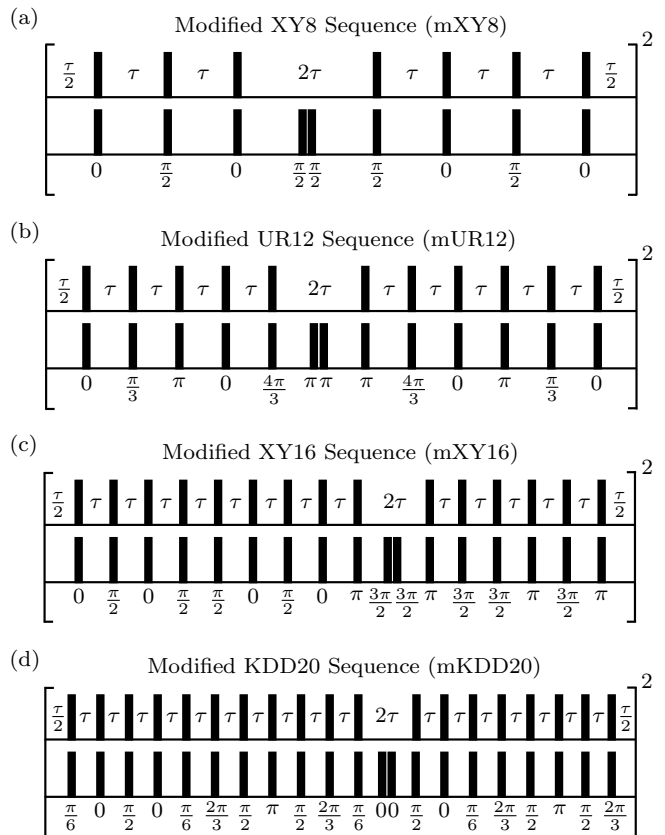


FIG. 2. Pulse sequences of the modified robust DD sequences for (a) mXY8 sequence, (b) mUR12 sequence, (c) mXY16 sequence, and (d) mKDD20 sequence, respectively. The sequence of pulses enclosed in brackets is performed twice to complete one cycle of the DD scheme, as indicated by the superscript 2. Each filled rectangle inside the brackets signifies a  $\pi$  pulse, with the axis about which these pulses are applied represented by the angles shown below each pulse. The duration of free evolution between two pulses is denoted by the parameter  $\tau$ .

### III. STATE PROTECTION USING DD SCHEMES

It is imperative to develop robust DD sequences that use a minimum number of pulses per cycle, with time delays between pulses and the phases of the pulses being the adjustable control parameters. Since standard DD sequences protected different orders of coherence to varying extents, we made modifications which were designed specifically for each different order of coherence.

Robust DD sequences use three distinct approaches to mitigate the effect of pulse imperfections, namely, (i) each  $\pi$  pulse is substituted with composite pulses, (ii) DD sequences are combined using XY4 as the base sequence, and (iii) optimal phases within the DD sequence are identified. Control pulses along both perpendicular axes,  $x$  and  $y$ , in the DD sequence ensure that coherence is equally preserved in both directions such sequences are associated with the XY family, including XY4, XY8, and

XY16 sequences [42, 49]. Another robust DD sequence, known as Knill Dynamical Decoupling (KDD), utilizes composite pulses, replacing a single  $\pi$  pulse along the  $\beta$  axis with five  $\pi$  pulses of distinct phases. An improved version of the KDD sequence is created by integrating the five-pulse  $\text{KDD}_\beta$  sequence into the XY4 dynamical decoupling (DD) sequence. This integration yields a twenty pulse DD sequence, the KDD20 sequence, with varying phases which preserves coherence along both the  $x$  and  $y$  axes. The family of URDD sequences represents another category of robust DD sequences, developed by finding optimal phases through a Taylor series expansion. The details of URDD sequences are provided in the references [50, 51].

Zero and second-order coherences are characterized by bipartite correlations that arise from the interactions between pairs of spins, and it is essential to protect the spins associated with these interactions. Often, standard robust DD sequences fail to preserve these coherences and hence these sequences were modified wherein, at a particular point ( $t_k$ ) selected close to the center of the sequence, the  $\pi$  pulse on the second qubit in the original DD sequence is substituted with two consecutive  $\pi$  pulses of the same phase (effectively creating a  $2\pi$  pulse). The first qubit in the meanwhile evolves freely for a duration of  $2\tau$ , where  $\tau$  is the interpulse delay. This modified sequence is executed twice (or for an even number of iterations) to confirm that the total impact of the sequence functions as the Identity operator. These modified DD sequences are generic and can be implemented on several different quantum hardware, as long the interpulse delays in the original sequence are kept uniform. In this study, four robust DD sequence were modified, and their corresponding pulse sequences are depicted in Figure 2.

#### IV. EXPERIMENTAL PROTECTION OF QUANTUM COHERENCE

A sample of  $^{13}\text{C}$  labeled diethylfluoromalonate was used to generate three-qubit quantum states with different coherence orders, with the  $^1\text{H}$ ,  $^{19}\text{F}$ , and  $^{13}\text{C}$ , spins serving as the first, second, and third qubits, respectively. Further details of the sample and its parameters are provided in the reference [52].

##### A. Zero order coherence

The dynamics of zero-order coherences were examined by experimentally generating two distinct quantum states with zero-order coherence, and their preservation against environmental noise was demonstrated using robust DD schemes. The states are given by:

$$|\psi_0^a\rangle = \frac{|010\rangle + |100\rangle}{\sqrt{2}}, \quad |\psi_0^b\rangle = \frac{|011\rangle + |101\rangle}{\sqrt{2}} \quad (5)$$

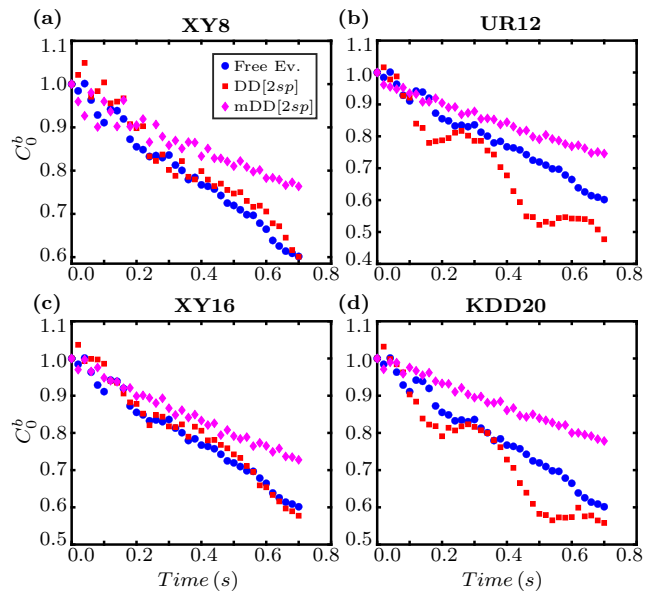


FIG. 3. Dynamics of zero-order coherence,  $C_0^b$  as a function of time, associated with the density matrix element  $\rho_{46}$  for the state  $|\psi_0^b\rangle$ , for the DD sequences: (a) XY8, (b) UR12, (c) XY16, and (d) KDD20. Pink diamonds and red squares denote the application of modified robust DD sequences (mDD[2sp]) and standard DD sequences (DD[2sp]), on the two spins, respectively. Blue circles denote the free evolution of zero-order coherence (Free Ev.).

Considering the density matrix formalism, the elements  $\rho_{35}$  and  $\rho_{46}$  are produced by the states  $|\psi_0^a\rangle$  and  $|\psi_0^b\rangle$ , respectively, which are associated with a magnetic quantum number of zero, and correspond to zero-order coherence. The state  $|\psi_0^a\rangle$  is experimentally prepared through a series of quantum gates, beginning with a Hadamard gate on the first qubit and a NOT gate on the second qubit. Subsequently, a  $\text{CNOT}_{12}$  gate is applied to the first two qubits, and during this process, the third qubit stays unaffected. The same set of gates are used to create the state  $|\psi_0^b\rangle$ , with the only difference being that the third qubit undergoes a NOT gate operation. The reconstructed density matrices associated with the states  $|\psi_0^a\rangle$  and  $|\psi_0^b\rangle$  had high measured experimental fidelities of 0.984 and 0.978, respectively. The evolution of the zero-order coherence is monitored at various time points via a single  $IYI$  pulse on the second qubit.

The zero-order coherences were subsequently protected by applying four standard DD sequences namely, XY8, UR12, XY16, and KDD20 and their modified versions namely, mXY8, mUR12, mXY16, and mKDD20. Interpulse delays for the modified sequences mXY8, mUR12, mXY16, and mKDD20 were set to 0.538 ms, 0.332 ms, 0.541 ms, and 0.417 ms respectively, for the state  $|\psi_0^a\rangle$  and to 0.515 ms, 0.331 ms, 0.540 ms, and 0.418 ms respectively, for the state  $|\psi_0^b\rangle$ . For both states, the interpulse delays are set to maintain a cycle duration of 0.01 seconds for the mXY16 and mKDD20 sequences, which includes the duration of the  $\pi$  pulses. In contrast, the

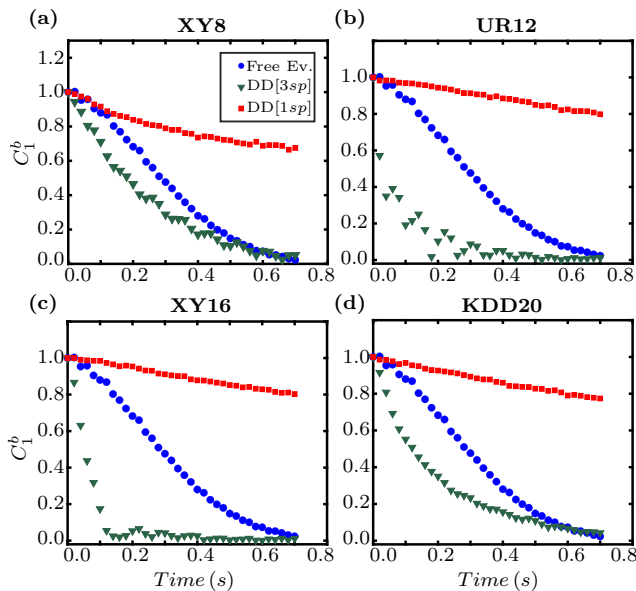


FIG. 4. Dynamics of first-order coherence,  $C_1^b$  as a function of time, associated with the density matrix element  $\rho_{78}$  for the state  $|\psi_1^b\rangle$ , after applying the DD sequences: (a) XY8, (b) UR12, (c) XY16, and (d) KDD20. Red squares and inverted green triangles denote the application of these DD sequences to a single qubit (DD[1sp]), and simultaneously on all three qubits (DD[3sp]), respectively. Blue circles denote the free evolution of first-order coherence (Free Ev.).

cycle duration for the mXY8 and mUR12 dynamical decoupling sequences is set at 0.005 seconds, while taking into account the duration of the  $\pi$  pulses.

The results of free evolution and protection of the state  $|\psi_0^b\rangle$  using standard and modified robust DD sequences are depicted in Figure 3, respectively. The plots indicate that some level of protection for zero-order coherence is provided by all four modified versions of robust DD sequences, with the mKDD20 sequence proving to be the most effective among all DD sequences in preserving zero-order coherence. A similar pattern was observed for the state  $|\psi_0^a\rangle$  (plots not shown). Further, it can be clearly observed that zero-order coherence is not protected by the standard DD sequences.

### B. First order coherence

Two quantum states that exhibit first-order coherences were experimentally generated and subsequently protected using robust DD sequences applied only on a single qubit. The states are given by:

$$|\psi_1^a\rangle = \frac{|000\rangle + |010\rangle}{\sqrt{2}}, \quad |\psi_1^b\rangle = \frac{|110\rangle + |111\rangle}{\sqrt{2}} \quad (6)$$

The density matrix elements  $\rho_{13}$  and  $\rho_{78}$  are associated with the quantum states  $|\psi_1^a\rangle$  and  $|\psi_1^b\rangle$ , respectively, with a magnetic quantum number of one.

The state  $|\psi_1^a\rangle$  is experimentally generated through the application of a single-qubit Hadamard gate on the second qubit, while the state  $|\psi_1^b\rangle$  is created by the application of single-qubit NOT gates on both the first and second qubits, followed by a Hadamard gate on the third qubit. The reconstructed density matrices associated with the states  $|\psi_1^a\rangle$  and  $|\psi_1^b\rangle$  had high experimental fidelities of 0.99 and 0.985, respectively. In NMR, first-order coherences can be directly measured without applying a detection pulse.

The first-order coherences were subsequently protected by applying robust DD sequences on the single qubit responsible for generating the specific first-order coherence. The interpulse delays were set to 0.58 ms, 0.789 ms, 0.58 ms, and 0.478 ms, and to 0.594 ms, 0.802 ms, 0.594 ms, and 0.468 ms, for the XY8, UR12, XY16, and KDD20 sequences, for the states  $|\psi_1^a\rangle$  and  $|\psi_1^b\rangle$ , respectively. For both states, the interpulse delays were chosen to guarantee that the total duration of one cycle is 0.005 seconds for the XY8 sequence and 0.01 seconds for the UR12, XY16, and KDD20 sequences, respectively.

The standard technique to preserve a three-qubit state consists of implementing a DD sequence on all three qubits simultaneously. The effectiveness of this method was compared with protection sequences applied to single qubits alone, focusing on the qubit responsible for generating first-order coherence. The results are displayed in Figure 4, corresponding to the state  $|\psi_1^b\rangle$ . The results suggest that all four robust DD sequences, specifically, XY8, UR12, XY16, and KDD20 successfully enhance the preservation of first-order coherence for the state over extended time periods when applied to a single qubit. The UR12 stands out as the most effective in preserving first-order coherence. In contrast, the standard approach of implementing DD sequences on all three qubits simultaneously leads to a fast deterioration of first-order coherence instead of preserving it. A similar pattern was observed for the state  $|\psi_0^a\rangle$  (plots not shown).

### C. Second order coherence

To investigate the dynamics of second-order coherences, two different three-qubit quantum states were experimentally created, given by:

$$|\psi_2^a\rangle = \frac{|000\rangle + |110\rangle}{\sqrt{2}}, \quad |\psi_2^b\rangle = \frac{|001\rangle + |111\rangle}{\sqrt{2}} \quad (7)$$

The states  $|\psi_2^a\rangle$  and  $|\psi_2^b\rangle$  correspond to the density matrix elements  $\rho_{17}$  and  $\rho_{28}$ , respectively, with a total magnetic quantum number of two.

The state  $|\psi_2^a\rangle$  is experimentally created by applying a Hadamard gate on the first qubit, followed by a CNOT<sub>12</sub> gate and no operation is performed on the third qubit. The same sequence of gates is employed to create the state  $|\psi_2^b\rangle$ , with an additional NOT gate on the third qubit. The reconstructed density matrices corresponding to the states  $|\psi_2^a\rangle$  and  $|\psi_2^b\rangle$  had measured experimental

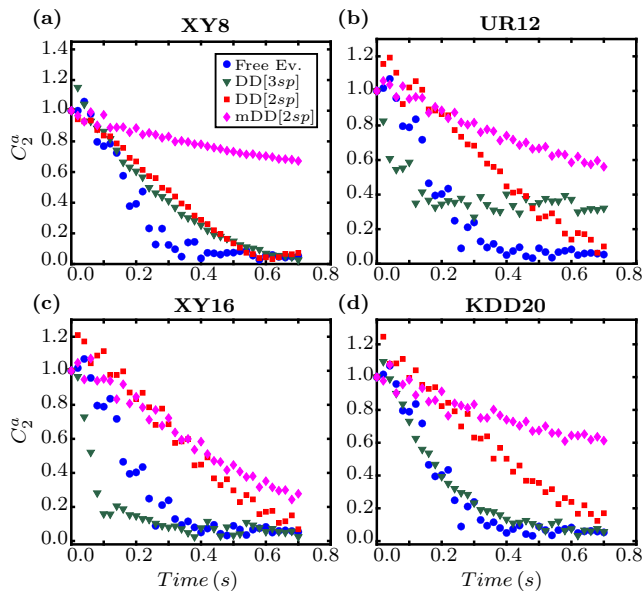


FIG. 5. Dynamics of second-order coherence,  $C_2^a$ , as a function of time associated with the density matrix element  $\rho_{17}$  for the state  $|\psi_2^a\rangle$ , after applying the DD sequences: (a) XY8, (b) UR12, (c) XY16, and (d) KDD20. Pink diamonds, red squares and inverted green triangles denote the application of modified (mDD[2sp]) and standard (DD[2sp]) DD sequences on the two relevant qubits, and simultaneously on all three qubits (DD[3sp]), respectively. Blue circles denote the free evolution of first-order coherence (Free Ev.).

Fidelities of 0.969 and 0.972, respectively. The dynamics of both states are tracked by performing direct measurements at different time points, utilizing a  $YII$  pulse applied to the second qubit. For both states, the interpulse delay between successive  $\pi$  pulses was set to 0.538 ms, 0.332 ms, 0.562 ms, and 0.417 ms for the mXY8, mUR12, mXY16, and mKDD20 sequences, respectively. The duration of one cycle of the DD sequence was set to 0.01 seconds for the mXY16 and mKDD20 sequences, and to 0.005 seconds for the mXY8 and mUR12 sequences respectively, which includes the time allocated for the  $\pi$  pulses.

The results of protection of second-order coherences in the state  $|\psi_2^a\rangle$  using standard and modified robust DD sequences are presented in Figure 5, which indicate that second-order coherence is successfully preserved for a longer duration when applying modified robust DD sequences. The mXY8 sequence stands out as the most successful in preserving second-order coherence. In contrast, implementing standard robust DD sequences provides only limited protection for second-order coherence. Further, the simultaneous application of standard DD sequences on all three qubits leads to a rapid degradation of second-order coherence rather than preserving it. A similar pattern was observed for the state  $|\psi_0^b\rangle$  (plots not shown).

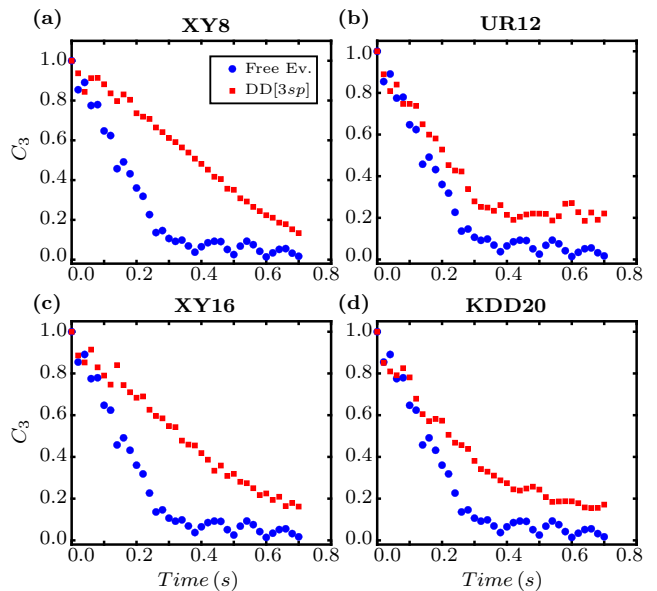


FIG. 6. Dynamics of third-order coherence,  $C_3$ , associated with the density matrix element  $\rho_{18}$  of the state  $|\psi_3\rangle$  after applying the DD sequences: (a) XY8, (b) UR12, (c) XY16, and (d) KDD20. Blue circles represent the Dynamics of third-order coherence during free evolution (Free Ev.) are denoted by blue circles, while red squares indicate the dynamics of after applying standard robust DD sequences on all three qubits.

#### D. Third order coherence

The highest order of coherence in a three-qubit system is of third order with a total magnetic quantum number of 3, corresponding to the  $\rho_{18}$  of the density matrix given by:

$$|\psi_3\rangle = \frac{|000\rangle + |111\rangle}{\sqrt{2}} \quad (8)$$

Third-order coherence is prepared experimentally by applying a Hadamard gate on the first qubit, immediately after which a CNOT gate (CNOT<sub>12</sub>) is applied that induces an interaction between the first and second qubits. Subsequently, a second CNOT gate (CNOT<sub>13</sub>) is applied, generating an interaction between the first and third qubits. The reconstructed density matrix for the state  $|\psi_3\rangle$  had an experimental fidelity of 0.97. An  $IYY$  pulse is applied to the second and third qubits to measure third-order coherence. The results of protection of third-order coherence after applying standard DD sequences are illustrated in Figure 6, indicating that all four DD sequences were able to successfully preserve third-order coherence to a good extent, with the highest efficacy in preserving it exhibited by the UR12 sequence.

Tables I-II display the percentage of zero and second-order coherences, and first and third-order coherences, respectively, which are protected after applying various robust DD sequences. As is evident, different robust DD

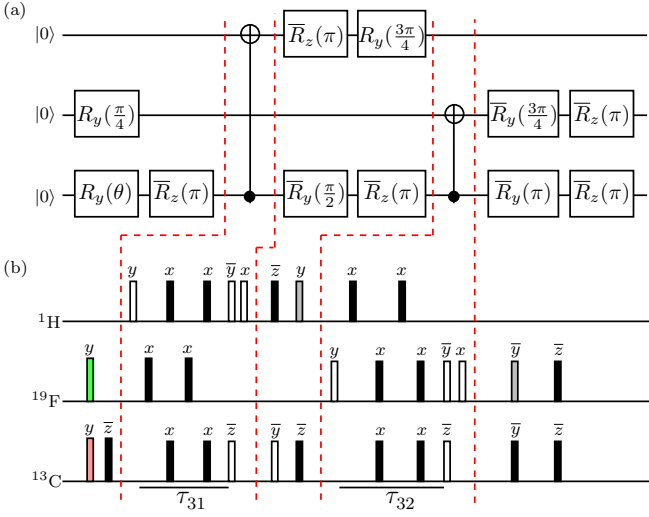


FIG. 7. (a) Quantum circuit to create a three-qubit star state, with  $R_\alpha(\beta)$  representing a single-qubit rotation gate of rotation angle  $\beta$  around the  $\alpha$  axis. (b) NMR pulse sequences to implement the quantum circuit. Filled and unfilled rectangles represent  $\pi$  and  $\pi/2$  radiofrequency (rf) pulses, respectively. The phase of each rf pulse is mentioned above it, with a bar indicating a negative phase. The parameters  $\tau_{31}$  and  $\tau_{32}$  correspond to the free evolution time periods,  $1/(2J_{31})$  and  $1/(2J_{32})$ , respectively; with the scalar coupling strength between qubits  $i$  and  $j$  being represented by  $J_{ij}$ .

TABLE I. The percentage of zeroth and second-order coherence preserved after applying modified versions of robust DD sequences (mXY8, mUR12, mXY16, and mKDD20) at 0.7 seconds, as well as during free evolution (Free Evo.) at the same time (0.7 seconds) where the maximal percentage of coherence preservation for each state is highlighted in red.

DD Seq.	$ \psi_0^a\rangle$	$ \psi_0^b\rangle$	$ \psi_2^a\rangle$	$ \psi_2^b\rangle$
mXY8	73.44%	76.36%	<b>67.18%</b>	<b>63.99%</b>
mUR12	75.46%	74.58%	56.12%	53.18%
mXY16	71.87%	72.77%	27.73%	26.03%
mKDD20	<b>76.26%</b>	<b>77.83%</b>	61.26%	63.56%
Free Evo.	63.35%	60.16%	0.522%	0.519%

TABLE II. The percentage of first and third-order coherence protected after the application of robust dynamical decoupling sequences (XY8, UR12, XY16, and KDD20) at 0.7 seconds, as well as during free evolution (Free Evo.) at the same time, is presented, with the maximum coherence preservation for each state highlighted in red.

DD Seq.	$ \psi_1^a\rangle$	$ \psi_1^b\rangle$	$ \psi_3\rangle$
XY8	63.94%	67.5%	13.35%
UR12	<b>76.35%</b>	<b>80.29%</b>	<b>22.09%</b>
XY16	73.17%	79.81%	16.20%
KDD20	70.64%	77.38%	17.14%
Free Evo.	0.603%	0.236%	0.17%

sequences are able to protect coherences of different orders to varying extents.

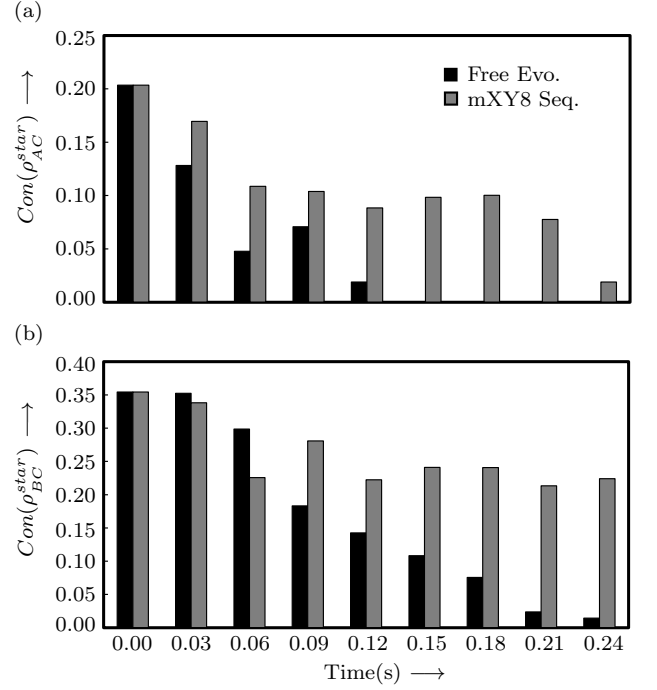


FIG. 8. Bar plots depicting the dynamics of entanglement, measured by concurrence values,  $Con(\rho_{AC}^{star})$  and  $Con(\rho_{BC}^{star})$  for the two-qubit subsystems of a three-qubit star state for (a)  $\rho_{AC}^{star}$  and (b)  $\rho_{BC}^{star}$ . The black solid bars indicate concurrence values when the states evolve under free evolution (Free Evo.), while gray solid bars represent the concurrence values when a modified XY8 DD sequence is applied (mXY8 Seq.).

## V. EXPERIMENTAL PROTECTION OF TWO-QUBIT ENTANGLEMENT IN A THREE-QUBIT STAR STATE

A three-qubit star state contains all possible orders of coherences, and we use the insights gained from using modified robust DD sequences for separately protecting different orders of coherence, to protect two-qubit entanglement present in a three-qubit star state.

A three-qubit star state was generated on the  $^{13}\text{C}$  labeled diethylfluoromalonate sample using the quantum circuit depicted in Figure 7(a), where  $R_\alpha(\beta)$  indicates a single-qubit rotation gate that performs a rotation of an angle  $\beta$  around the  $\alpha$  axis. The NMR pulse sequence corresponding to this circuit is shown in Figure 7(b). State tomography was carried out to reconstruct the density matrix, with a computed fidelity of 0.92. Subsequent to star state  $|\psi^{star}\rangle$  preparation, the modified XY8 (mXY8) DD sequence was utilized to protect the entanglement in the two-qubit subsystems  $\rho_{AC}^{star}$  and  $\rho_{BC}^{star}$ . The mXY8 DD sequence was applied on qubits 1 and 3, for the state  $\rho_{AC}^{star}$ , and on qubits 2 and 3, for the state  $\rho_{BC}^{star}$ , with the duration of interpulse delay fixed to 0.563 ms and 0.540 ms, respectively. This ensures that the duration of one full cycle of the mXY8 sequence is 0.005 seconds, incorporating the duration of  $\pi$  pulses. Complete

state tomography was performed, involving seven sets of pulses, namely,  $III$ ,  $IYY$ ,  $IYY$ ,  $YII$ ,  $XYX$ ,  $XXY$  and  $XXX$ , to reconstruct the entire density matrix of the star state. Finally, qubit 2 and qubit 1 were traced out to produce the two-qubit reduced density matrices,  $\rho_{AC}^{star}$  and  $\rho_{BC}^{star}$ , respectively. The evolution of entanglement in these states are examined by evaluating the concurrence, both during free evolution and when the mXY8 DD sequences are applied. The results are presented in Figure 8, which clearly indicates that the modified mXY8 DD sequences have successfully preserved the two-qubit entanglement in the two subsystems of the three-qubit star state.

## VI. CONCLUSIONS

Different orders of coherence were generated in three NMR qubits and their behavior studied during free evolution and after implementing robust DD protection schemes. While standard DD sequences are able to successfully protect third-order coherence, other coherence orders deteriorate rapidly and are not protected. Hence the standard robust DD sequences were applied solely to a single qubit for the protection of first-order coherences. The experimental results indicate that first-order coherences are effectively protected, while for the remain-

ing coherence orders, the standard DD sequences were suitably modified. These modified sequences are very effective in preserving zero-order and second-order coherences when applied to the two spins involved in generating these coherences. Our results indicate that overall state fidelity after applying a specific DD sequence might not be the best way to judge the efficacy of state protection, and also opens up avenues to explore the protection of specific coherence orders. Finally, the entanglement in two-qubit subsystems of a three-qubit star state was protected by applying these modified sequences. The presence of entanglement was monitored by evaluating concurrence and the experiments revealed that the modified version XY8 DD sequence effectively protects entanglement in the two-qubit subsystems,  $\rho_{AC}^{star}$  and  $\rho_{BC}^{star}$ , for a longer duration. Future extensions of this work involve the development of robust DD sequences for multiqubit systems to simultaneously protect the various orders of coherences.

## ACKNOWLEDGMENTS

All the experiments were performed on a Bruker Avance-III 600 MHz FT-NMR spectrometer at the NMR Research Facility of IISER Mohali.

- 
- [1] M. A. Nielsen and I. L. Chuang, *Quantum Computation and Quantum Information* (Cambridge University Press, 2000).
  - [2] F. Ahnefeld, T. Theurer, D. Egloff, J. M. Matera, and M. B. Plenio, *Phys. Rev. Lett.* **129**, 120501 (2022).
  - [3] J. Ma, Y. Zhou, X. Yuan, and X. Ma, *Phys. Rev. A* **99**, 062325 (2019).
  - [4] V. Giovannetti, S. Lloyd, and L. Maccone, *Nat. Photonics* **5**, 222–229 (2011).
  - [5] J. Åberg, *Phys. Rev. Lett.* **113**, 150402 (2014).
  - [6] M. Lostaglio, D. Jennings, and T. Rudolph, *Nat. Commun.* **6**, 6383 (2015).
  - [7] V. Narasimhachar and G. Gour, *Nat. Commun.* **6**, 7689 (2015).
  - [8] C.-M. Li, N. Lambert, Y.-N. Chen, G.-Y. Chen, and F. Nori, *Sci. Rep.* **2**, 885 (2012).
  - [9] D. G. Cory, A. F. Fahmy, and T. F. Havel, *Proc. Nat. Acad. Sci.* **94**, 1634–1639 (1997).
  - [10] N. A. Gershenfeld and I. L. Chuang, *Science* **275**, 350–356 (1997).
  - [11] M. H. Devoret and R. J. Schoelkopf, *Science* **339**, 1169–1174 (2013).
  - [12] J. Clarke and F. K. Wilhelm, *Nature* **453**, 1031 (2008).
  - [13] E. Romero, R. Augulis, V. I. Novoderezhkin, M. Ferretti, J. Thieme, D. Zigmantas, and R. van Grondelle, *Nat. Photonics* **10**, 676–682 (2014).
  - [14] E. M. Gauger, E. Rieper, J. J. L. Morton, S. C. Benjamin, and V. Vedral, *Phys. Rev. Lett.* **106**, 040503 (2011).
  - [15] J. A. Pauls, Y. Zhang, G. P. Berman, and S. Kais, *Phys. Rev. E* **87**, 062704 (2013).
  - [16] J. N. Bandyopadhyay, T. Paterek, and D. Kaszlikowski, *Phys. Rev. Lett.* **109**, 110502 (2012).
  - [17] T. Baumgratz, M. Cramer, and M. B. Plenio, *Phys. Rev. Lett.* **113**, 140401 (2014).
  - [18] T. R. Bromley, M. Cianciaruso, and G. Adesso, *Phys. Rev. Lett.* **114**, 210401 (2015).
  - [19] C. Napoli, T. R. Bromley, M. Cianciaruso, M. Piani, N. Johnston, and G. Adesso, *Phys. Rev. Lett.* **116**, 150502 (2016).
  - [20] A. Streltsov, U. Singh, H. S. Dhar, M. N. Bera, and G. Adesso, *Phys. Rev. Lett.* **115**, 020403 (2015).
  - [21] S. Kim, C. Xiong, S. Luo, A. Kumar, and J. Wu, *Phys. Rev. A* **108**, 012416 (2023).
  - [22] J. Ma, B. Yadin, D. Girolami, V. Vedral, and M. Gu, *Phys. Rev. Lett.* **116**, 160407 (2016).
  - [23] C. L. Liu and D. L. Zhou, *Phys. Rev. Lett.* **123**, 070402 (2019).
  - [24] B. Regula, K. Fang, X. Wang, and G. Adesso, *Phys. Rev. Lett.* **121**, 010401 (2018).
  - [25] I. Marvian and R. W. Spekkens, *Phys. Rev. A* **94**, 052324 (2016).
  - [26] I. S. Oliveira, T. J. Bonagamba, R. S. Sarthour, J. C. C. Freitas, and E. R. deAzevedo, *NMR Quantum Information Processing* (Elsevier, Linacre House, Jordan Hill, Oxford OX2 8DP, UK, 2007).
  - [27] D. P. Pires, I. A. Silva, E. R. deAzevedo, D. O. Soares-Pinto, and J. G. Filgueiras, *Phys. Rev. A* **98**, 032101 (2018).
  - [28] D. Dhar, L. K. Grover, and S. M. Roy, *Phys. Rev. Lett.* **96**, 100405 (2006).



- [29] A. Basit, F. Badshah, H. Ali, and G.-Q. Ge, *Europhys. Lett.* **118**, 30002 (2017).
- [30] S.-C. Wang, Z.-W. Yu, W.-J. Zou, and X.-B. Wang, *Phys. Rev. A* **89**, 022318 (2014).
- [31] E. Knill and R. Laflamme, *Phys. Rev. A* **55**, 900 (1997).
- [32] L.-M. Duan and G.-C. Guo, *Phys. Rev. Lett.* **79**, 1953 (1997).
- [33] L. Viola and E. Knill, *Phys. Rev. Lett.* **94**, 060502 (2005).
- [34] W. Yang and R.-B. Liu, *Phys. Rev. Lett.* **101**, 180403 (2008).
- [35] G. S. Uhrig, *Phys. Rev. Lett.* **102**, 120502 (2009).
- [36] L. P. Pryadko and G. Quiroz, *Phys. Rev. A* **80**, 042317 (2009).
- [37] J. Du, X. Rong, N. Zhao, Y. Wang, J. Yang, and R. B. Liu, *Nature* **461**, 1265 (2009).
- [38] Y. Wang, X. Rong, P. Feng, W. Xu, B. Chong, J.-H. Su, J. Gong, and J. Du, *Phys. Rev. Lett.* **106**, 040501 (2011).
- [39] M. J. Biercuk, H. Uys, A. P. VanDevender, N. Shiga, W. M. Itano, and J. J. Bollinger, *Phys. Rev. A* **79**, 062324 (2009).
- [40] S. S. Roy, T. S. Mahesh, and G. S. Agarwal, *Phys. Rev. A* **83**, 062326 (2011).
- [41] Q.-Y. Cao, P.-C. Yang, M.-S. Gong, M. Yu, A. Retzker, M. Plenio, C. Müller, N. Tomek, B. Naydenov, L. McGuinness, F. Jelezko, and J.-M. Cai, *Phys. Rev. Appl.* **13**, 024021 (2020).
- [42] M. A. Ali Ahmed, G. A. Álvarez, and D. Suter, *Phys. Rev. A* **87**, 042309 (2013).
- [43] X.-L. Zhen, F.-H. Zhang, G. Feng, H. Li, and G.-L. Long, *Phys. Rev. A* **93**, 022304 (2016).
- [44] H. Singh, Arvind, and K. Dorai, *Phys. Rev. A* **90**, 052329 (2014).
- [45] H. Singh, Arvind, and K. Dorai, *Europhysics Letters* **118**, 50001 (2017).
- [46] H. Cao, C. Radhakrishnan, M. Su, M. M. Ali, C. Zhang, Y.-F. Huang, T. Byrnes, C.-F. Li, and G.-C. Guo, *Phys. Rev. A* **102**, 012403 (2020).
- [47] K. Dorai and A. Kumar, *Journal of Magnetic Resonance, Series A* **114**, 155 (1995).
- [48] K. Dorai, T. S. Mahesh, Arvind, and A. Kumar, *Current Science* **79**, 1447 (2000).
- [49] G. A. Álvarez, A. M. Souza, and D. Suter, *Phys. Rev. A* **85**, 052324 (2012).
- [50] G. T. Genov, D. Schraft, N. V. Vitanov, and T. Halfmann, *Phys. Rev. Lett.* **118**, 133202 (2017).
- [51] A. Gautam, Arvind, and K. Dorai, *Int. J. Quantum Inform.* **21**, 2350016 (2023).
- [52] A. Gautam, K. Dorai, and Arvind, *Quant. Inf. Proc.* **21**, 329 (2022).